Journal of Molecular Structure 1074 (2014) 534–541

Contents lists available at ScienceDirect

Journal of Molecular Structure

journal homepage: www.elsevier.com/locate/molstruc

# Electronic properties of hyperbranched compounds derived by pyrrole

Lioudmila Fomina [a,*], Jorge Godínez Sánchez [b], J.A. Olivares [c], F.L.S. Cuppo [c], L. Enrique Sansores [a], Roberto Salcedo [a]

[a] Instituto de Investigaciones en Materiales, Universidad Nacional Autónoma de México, Circuito exterior s/n, Ciudad Universitaria Coyoacán 04510, México, DF, Mexico
[b] Escuela Nacional Preparatoria No 3, Justo Sierra, Universidad Nacional Autónoma de México, Av. Ing. Eduardo Molina No 1577, Gustavo A. Madero, 07400 México, DF, Mexico
[c] Centro de Investigación en Polímeros, Marcos Achar Lobaton No. 2 Tepexpan, 55885 México, Mexico

## HIGHLIGHTS

- Hyperbranched molecules containing pyrrole units were synthetized.
- These hyperbranched molecules show large electronic delocalization.
- Theoretical results show that para-hyperbranched polymer has an uncommon symmetry.
- The conductivity measurements indicated an energy band gap of 0.2 eV.
- Microscopy studies identify two phases where self-assembling is important.

## GRAPHICAL ABSTRACT

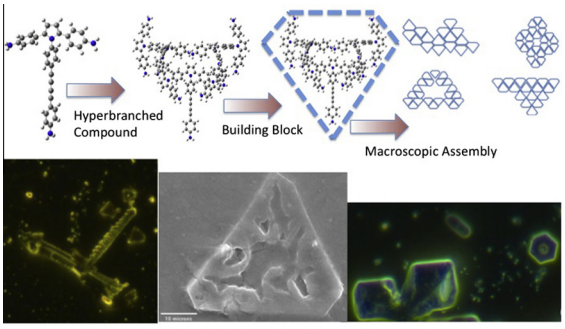


Macroscopic Morphologies from Hyperbranched Compound

## ARTICLE INFO

*Article history:*
Received 18 March 2014
Received in revised form 7 June 2014
Accepted 9 June 2014
Available online 19 June 2014

*Keywords:*
Hyperbranched polymers
Electronic properties
Diacetylenes
Semiconducting polymers
Morphology

## ABSTRACT

The electronic structure of hyperbranched polymers obtained from para-diaminodiphenyldiacetylenes as $AB_2$ type monomers by one-step polymerization is studied using DFT calculations. Five generations are modelled with optimization at each step. As the molecule grows it shows a helical shape conserving the C2 symmetry with wing like fragments covering the backbone. There is accidental degeneracy of the HOMO with the HOMO-1 and of the HOMO-2 with the HOMO-3. The LUMO is always located at the backbone and the HOMO set at the dianyline-pyrrole fragment. The HOMO–LUMO gap decreases as the molecule grows. Conductivity measurements as well as microscopy studies of para-hyperbranched polymer were carried out. Conductivity measurements as a function of temperature show semiconductor behavior. Optical microscopy reveals a macroscopic crystalline structure of this hyperbranched polymer.


## Introduction

The dendrimeric polymers can be classified into three large groups [1]: the first one refers specifically to the basic dendrimers i.e. molecules which grow in branches [2] and they are prepared in steps; the second group is formed by the so called dendro-injerted polymers [3] which have been described as the intermediated species between the dendrimers and the hyperbranched polymers; and the third group is constituted by the hyperbranched polymers [4,5]. There are several species that belong to the third group [6]. They are very interesting substances with highly branched structures, three dimensional architecture, globular shape, terminal functional groups and particular electronic behavior [5]; they can be prepared by polymerization in one or several steps synthesis [6].

The diacetylene derivatives shown in this communication belong to this group. Recently, hyperbranched molecules containing pyrrole units were obtained by Godínez Sánchez et al. [6] from ortho-, meta- and para-diaminodiphenyldiacetylenes as $AB_2$ type monomers by one-step polymerization. The new compounds can

* Corresponding author. Tel.: +52 5556224727.
*E-mail address:* lioudmilafomina@gmail.com (L. Fomina).

http://dx.doi.org/10.1016/j.molstruc.2014.06.031
0022-2860/

take orientations ortho, meta and para. All of them show a large electronic delocalization, which makes them important targets for high conductivity. Particularly, we will focus on the para analogue, which has a curious geometry that can give it a large way for electronic transport. This work is part of a research in which our group has published some interesting results [6–8].

In this paper we report the structural characterization of para-hyperbranched polymer and a theoretical study to understand the nature of its properties. The molecule of the para-hyperbranched compound is shown in Fig. 1 and its synthesis was reported in [6]. It has been previously characterized by means of infrared and NMR spectroscopy [9].

## Experimental part

### *Synthesis [6]*

#### *Synthesis of the monomer compound*

(1) 4-(*N*-Boc-amino)phenylacetylene. To a solution of di-tert-butyl dicarbonate ($BOC_2O$) (27.56 g, 126.28 mmol) in 42 mL THF, was added aminophenylacetylene (4.85 g, 41.39 mmol). Solution was stirred and refluxed for three hours. The solvent was removed in vacuum and the product was purified by column chromatography using hexane–ethyl acetate 10:1–5:1 as eluent.

(2) 4,4′-Di(*N*-Boc-amino)diphenyldiacetylene. To a solution of compound **1** (2.00 g, 9.2 mmol) in 20 mL isopropanol was added (0.025 g, 0.252 mmol) of copper chloride and 0.3 mL of N,N,N′,N′-tetramethylethylenediamine (TMEDA), the mixture was stirring under oxygen atmosphere for 3 h, and resulting solution was added to acidified water. The product was separated by filtration, dried in vacuum and purified by recrystallization from hexane.

(3) 4, 4′-Diaminodiphenyldiacetylene. To a suspension of 1.25 g (2.89 mmol) of compound **2** in 110 mL of MeOH was added 125 mL of concentrated HCl, and the mixture was stirred for 42 h at room temperature. The supernate was pipetted off, and the solid was stirred in 100 mL of acetone overnight, after which it was filtered off, washed four times with 15 mL of acetone, and pumped dry.

#### *Synthesis of para-hyperbranched compound*

Method **A**. A mixture of compound **3** (0.1 g, 0.43 mmol), copper (I) chloride (0.05 g, 0.5 mmol) in 10 mL dimethylformamide was refluxed under nitrogen for 24–48 h at 110 °C in an oil bath and allowed to cool to room temperature. The mixture was diluted with excess of acidified water. The precipitate was collected by filtration and dried in vacuum. Method **B**. A mixture of compound **3** (0.5 g, 2.15 mmol), copper (I) chloride (0.05 g, 0.5 mmol) in dioxane (10 mL) was refluxed under nitrogen for 24 h at 70 °C in an oil bath and allowed to cool to room temperature. The solution was diluted with excess of acidified water. The precipitate was collected by filtration and dried in vacuum.

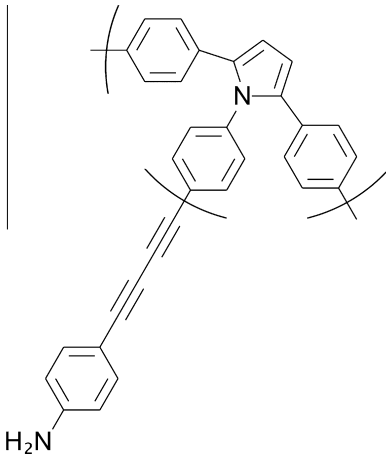


**Fig. 1.** Para-hyperbranched polymer.

#### *Electrical conductivity measurements*

The para-hyperbranched compound is partially soluble in acetone; however, it was not possible to produce a continuous homogenous film. The measurement of its conductivity was carried out as a powder sample in a specially designed cell. This cell consists of a transparent polystyrene tube, PSC, and two cylindrical steel electrodes with a diameter, $D = 3.19$ mm. The powder sample was pressed between the steel electrodes and the final samples thickness, $L = 1.46$ mm was measured with a Vernier scale (Fig. 2). Then the cell was placed inside a microscope hot stage adapted to heat uniformly the samples region. Conductivity measurements were carried out as a function of the temperature using and LCR meter. The measurements were carried out at 20 Hz frequency. The initial temperature was 10 °C and then the sample was heated at a ratio of 3.5 °C/min until a temperature of 50 °C was reached and cooled again at a ratio of 1 °C/min.

#### *Microscopy analysis*

The para-hyperbranched sample was observed by optical microscopy and scanning electron microscopy. Since the sample is partially soluble in acetone, two different samples were prepared. The first sample was a mixture of powder with deionized water (0.1% wt) and dispersed by 15 min in an ultrasonic bath. The second sample was prepared by mixing the powder sample in acetone to study the dissolved part of the para-hyperbranched polymer. Drops of these two samples were poured on clean glass slides and observed directly by optical microscopy. Different illumination techniques were used: bright field, polarize light and dark field to enhance the sample contrast with the glass substrate.

The sample for scanning electron microscopy (SEM) was prepared by pouring a drop from the deionized water mixture. After water evaporates, the sample was coated with a thin layer of gold for its observation under the SEM.

#### *Computational details*

All structures have been optimized at B3PW91/3-21G using the Gaussian09 code [10]. For all geometries, the starting point was a non-symmetric structure. For the third and fourth generation, before the last optimization the structure was very near $C_2$ symmetry, so we force to this symmetry and optimized again. The final structure with lower energy is $C_2$.

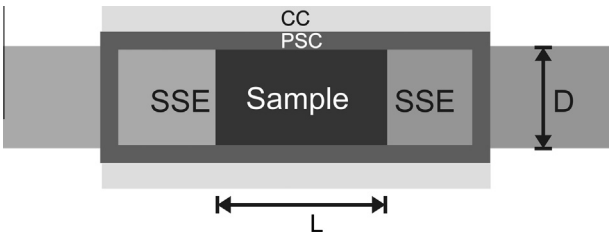


**Fig. 2.** Schematic cell for impedance measurements. Stainless Steel Cylindrical Electrodes (SSE), Transparent Polystyrene Tube (PSC), Semi Cylindrical Copper Cover (CC). The electrode radio is *D* and the sample thickness is *L*.

## Results

### *Synthesis*

*Monomer synthesis*

The synthetic route to the monomer **3** is shown in Figs. 3–5. This monomer was prepared from para-aminophenylacetylene, in three steps.

Terminal amino groups have been converted into N-Boc-amino groups by treating aminophenylacetylene with di-tert-butyl dicarbonate ($BOC_2O$) in THF (Fig. 3) in order to protect amino groups for the next reaction of oxidative coupling (Fig. 4).

Diyne compound **2** was obtained by a modified procedure of Hay's oxidative coupling using copper (I) chloride as a catalyst [8] (Fig. 4).

The protective groups were removed by treating compound **2** by concentrated HCl giving the resulting monomer **3** (Fig. 5) containing diacetylenic and terminate amino groups in 64–68% yield.

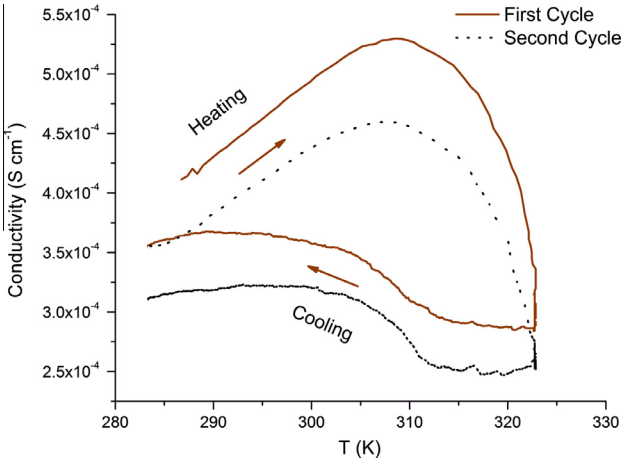


**Fig. 7.** Conductivity versus temperature for two cycles. Red Curve corresponds to the first cycle. (For interpretation of the references to color in this figure legend, the reader is referred to the web version of this article.)

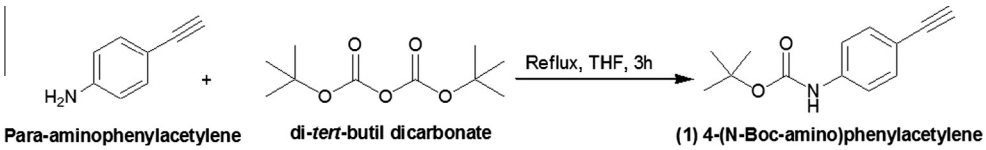


**Fig. 3.** Synthesis of 4-(*N*-Boc-amino)phenylacetylene (1).

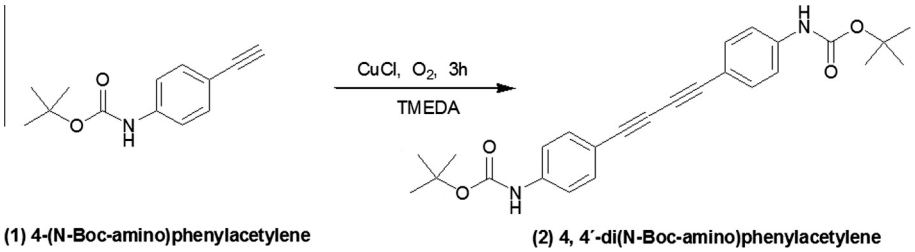


**Fig. 4.** Synthesis of 4,4′-di(N-Boc-amino)diphenyldiacetylene (2).

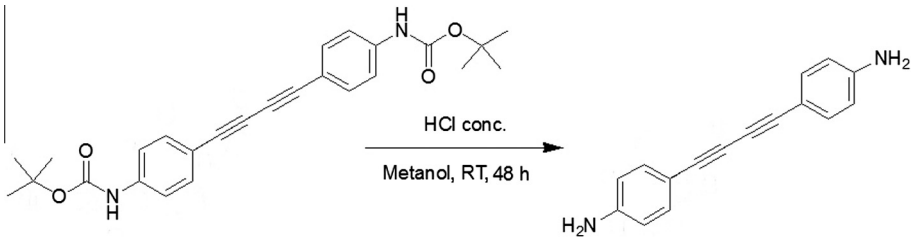


**Fig. 5.** Synthesis of 4,4′-diaminodiphenyldiacetylenes (3).

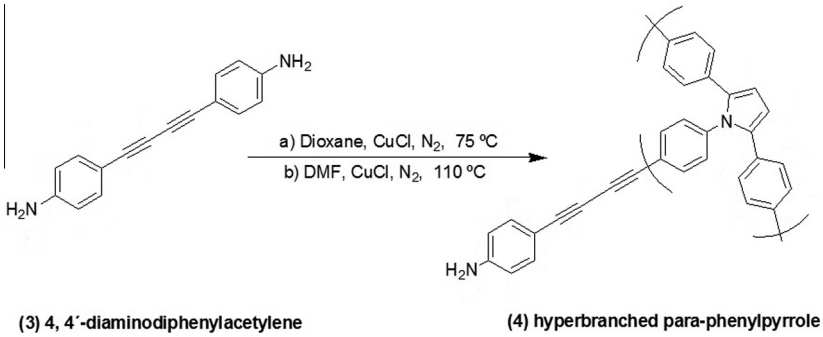


**Fig. 6.** Synthesis of para-hyperbranched molecule (4) from 4,4′-diaminodiphenyldiacetylene (3).

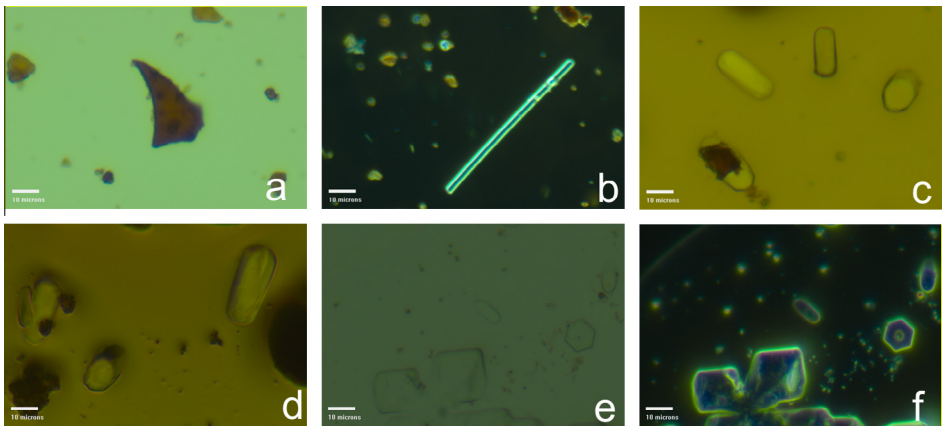


**Fig. 8.** Several morphologies founded by optical microscopy. Pictures from (a–f) were taken using bright field illumination. Picture (g) dark field illumination of (f). Picture (b) was taken between cross polarizers.

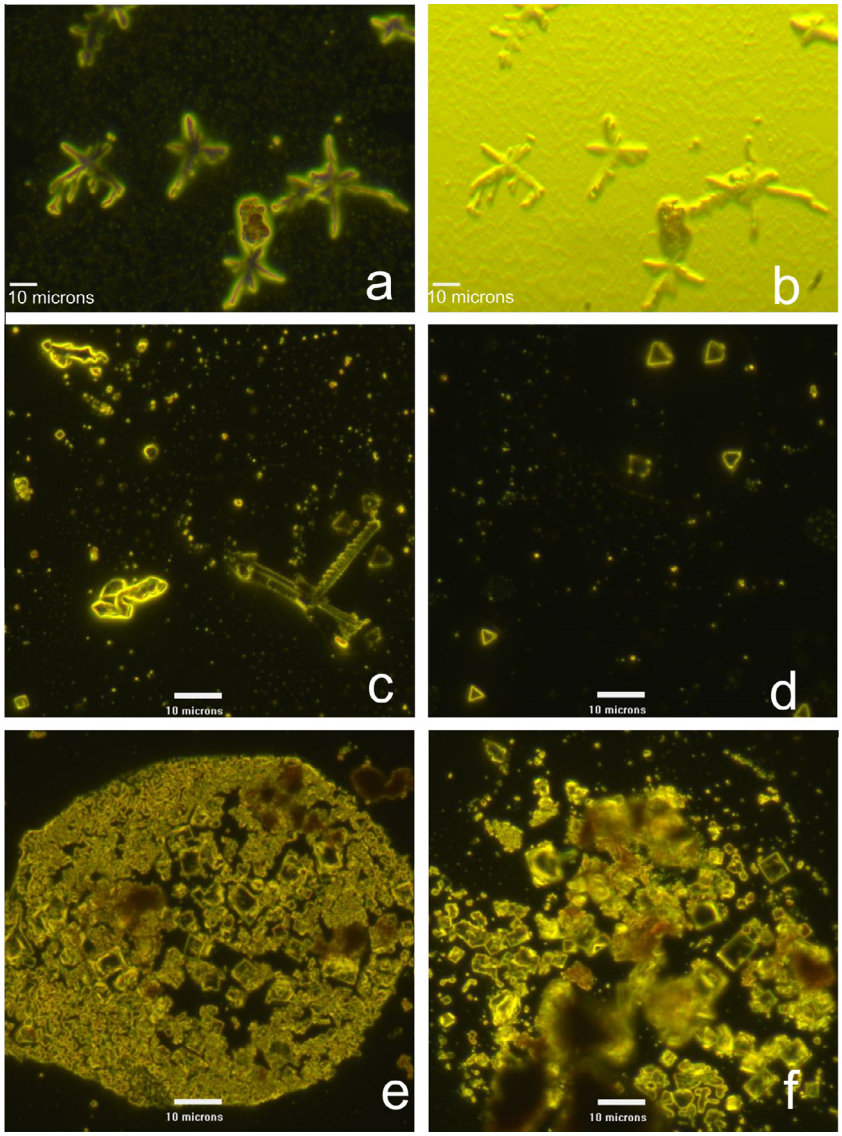


**Fig. 9.** Dark field microscopy of sample dissolved in acetone. In the figure it can be appreciated dendrimers as well as regular geometrical shapes.

*Polymerization*

Para-diaminodiphenyldiacetylene (**3**) as $AB_2$ type monomer was polymerized by two methods [8]. Method A – in DMF under nitrogen at 110 °C and method B – in dioxane under nitrogen at 70 °C using copper (I) chloride as catalyst in both cases (Fig. 6). Diacetylenic fragments and terminal amino groups reacted to yield pyrrole units. These reactions are carried out by one step polymerization.

The para-hyperbranched polymer was obtained from para-diaminodiphenyldiacetylene as $AB_2$ type monomer by one-step polymerization. Due to the method of synthesis of this compound we cannot to define a generation of this hyperbranched polymer. The prepared polymer should be considered as a mixture in which there are molecules of very different sizes, therefore, the general macroscopic properties as conductivity and morphology correspond to a response of all formed chains.

*Electrical conductivity measurements*

In Fig. 7, we show the two-cycle measurement of the conductivity, $\sigma$ as a function of the temperature. The sample presents a hysteresis behavior that can be related to polymer degradation with temperature. As a consequence, the conductivity values were reduced by 13% between the first and the second cycle. As can be noticed in Fig. 7, the samples conductivity increases with temperature in the range between $T = 283$ K and $T = 315$ K. This is a typical behavior of a semiconductor material. After $T = 315$ K the conductivity decreases following an ohmic behavior [11]. The activation energy, $E_a$, can be obtained by fitting $\sigma$ data in the semiconducting range, with the relation:

$$Ln\frac{\sigma}{\sigma_0} = -\frac{E_a}{2kT}, \quad (1)$$

where $k$ is the Boltzmann constant, $T$ the temperature in Kelvin and $\sigma_0$ the ideal conductivity for a monocrystalline structure [11]. The adjustment for each cycle gives the same activation energy, $E_a = 0.200$ +/− .003 eV, while $\sigma_0$ (S cm$^{-1}$) increases from 39.64 S cm$^{-1}$ in the first cycle to 52.45 S cm$^{-1}$ in the second cycle.

*Microscopy analysis*

Microscopy studies of para-hyperbranched polymer were carried out too. In Fig. 8(a)–(f) bright field illumination was used. For Fig. 8(b) the sample was placed between crossed polarizers for probing anisotropy domains. In Fig. 8(d) oblique illumination was used to enhance samples edges. Fig. 8(g) corresponds to the same sample of Fig. 8(f) using the dark field technique to enhance contrast at the edges.

Four different structures are relevant: amorphous flat structure (flakes) as in Fig. 8(a), tubular or cylindrical, Fig. 8(b), and ellipsoidal structures, Fig. 8(c) and (d). A crystalline structure with very sharp edges is seen in Fig. 8(f) and (g). The flake-like structures, Fig. 8(a), strongly absorb light and they appear always in yellowish tones. Other structures are transparent, neither presenting optical absorption nor refractive index contrast with the glass substrate. It is noticeable in Fig. 8(d)–(f) the presence of regular geometrical shapes. In Fig. 8(d) a solid cylinder appears while in Fig. 8(f) a perfect hexagonal cylindrical shape was found.

The highly geometrical shapes suggest that the soluble part of the sample has a crystalline structure with an optical anisotropy. To observe the formation of the crystal structure a drop of the

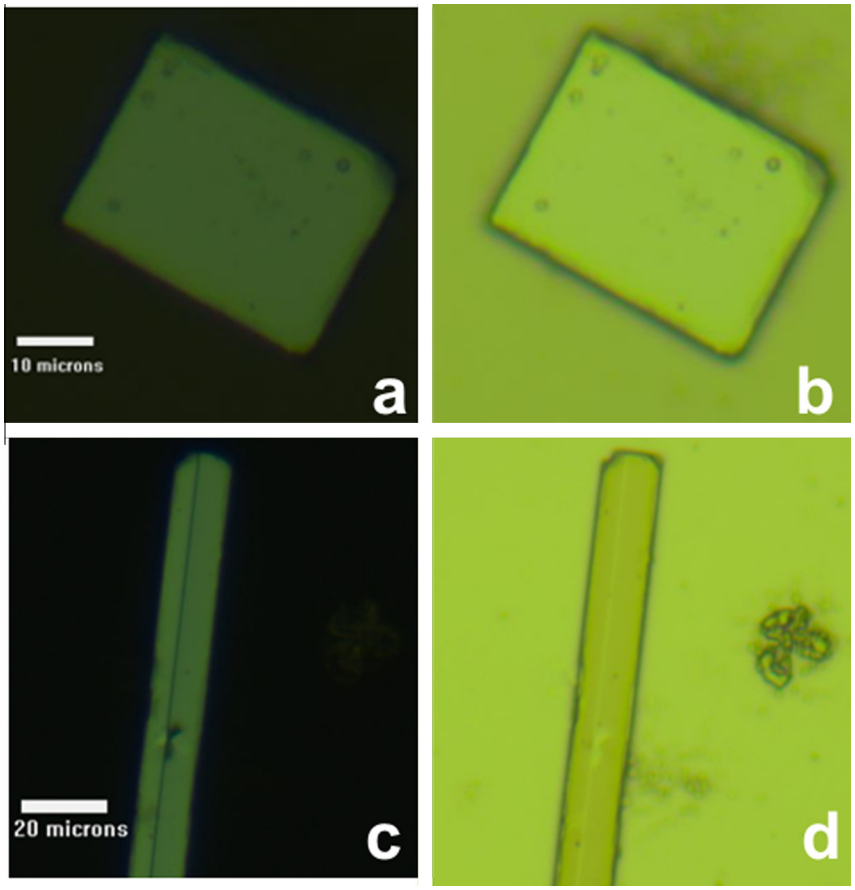


**Fig. 10.** Polarization microscopy. Optical anisotropy of the sample can be appreciated. Sample between cross polarizes and (a and c) and regular illumination, (b and d).

sample dissolved in acetone was placed on a clean glass slide and then we left the acetone to evaporate freely. Micrographs of this are shown in Figs. 9–11. In Fig. 9(a) a dendrimer structure is shown using dark field technique and its corresponding oblique illumination 9(b) to enhance the dendrimers volume. In Fig. 9(c) a dendrimer structure appears as well as some regular triangular shapes. In

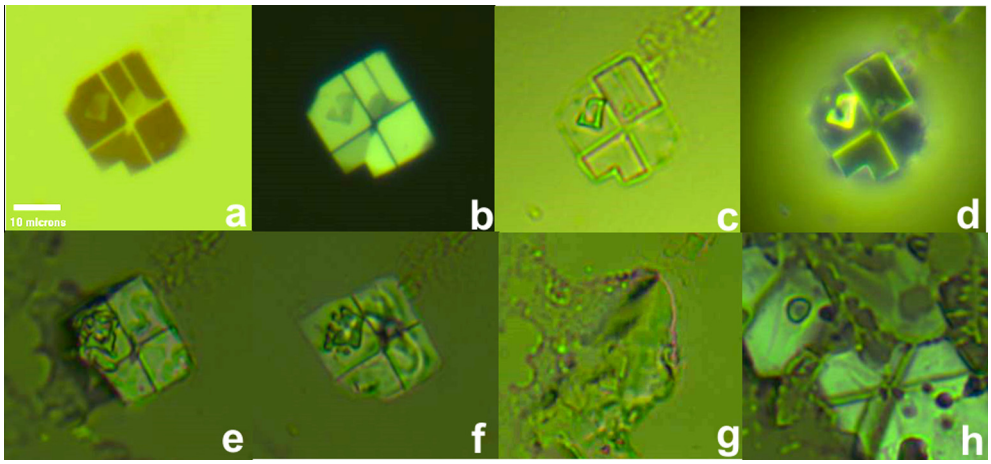


**Fig. 11.** Behavior of regular geometrical shape under different illuminations: (a–c) illuminated with polarized light. (d) Dark field illumination. (e–h) After a drop of acetone was pour on sample.

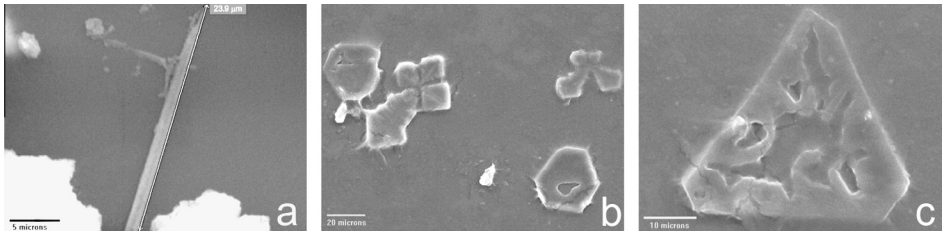


**Fig. 12.** SEM microscopy. It can be observed large tubes (a) rhomboids (b) and triangles (c).

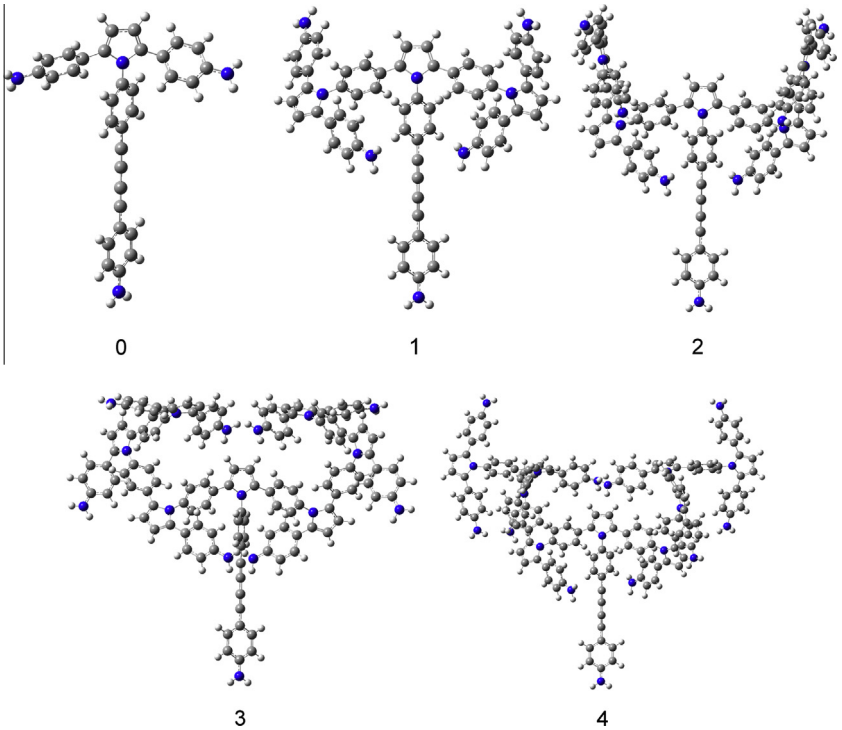


**Fig. 13.** Optimized geometries of the generations 0–4 of the para-hyperbranched polymer.

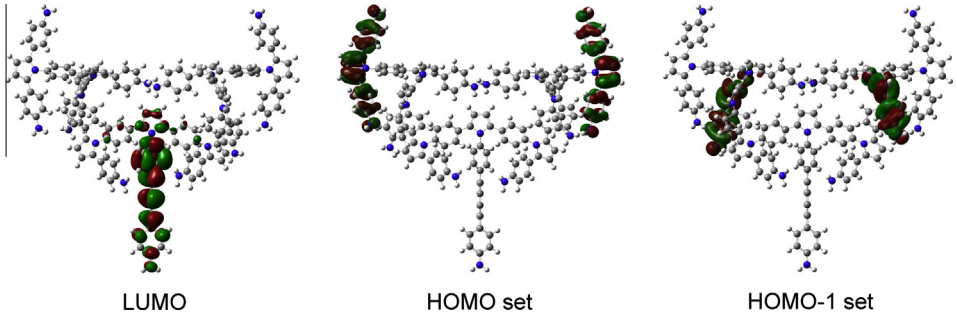


**Fig. 14.** Spatial representation of the LUMO, HOMO set and HOMO-1 set for generation 4.

Fig. 9(d) perfect isosceles triangles are displayed. Two regions of highly concentrated polymer were found and shown in Fig. 9(e) and (f), in which several regular parallelograms are displayed.

Some of the regular geometric shapes show birefringence when they are illuminated between crossed polarizers. This is an indicative of an optical uniaxial media. In Fig. 10 an isolated parallelogram and a rod-like structure with a square base are shown between cross polarizers, Fig. 10(a) and (c), and without analyzer in Fig. 10(b) and (d).

In Fig. 11 a curious four-domain structure is shown. The structure changes its color as the polarization of the incident light is rotated, Fig. 11(a)–(c). In Fig. 11(d) the sample is displayed under dark field technique. A drop of acetone was pour onto this structure, Fig. 11(e), its absorption by the polymer structure, Fig. 11(f) and (g) and the crystallization process as solvent evaporates, Fig. 11(h).

Fig. 12 shows photographs of the sample illuminated by SEM. Some of the previous structures observed in the optical microscope also appear. In Fig. 12(a) rod shape structure is observed as long as 25 μm and a thickness of 1.24 μm. In Fig. 12(b) some geometrical shapes similar to Fig. 8(g) are displayed. And in Fig. 12(c) an isosceles triangle is shown.

**Table 1**
Energy and symmetry of the frontier orbitals, HOMO–LUMO gap, total energy and dipole.

| Generation | | 0 | 1 | 2 | 3 | 4 |
|---|---|---|---|---|---|---|
| LUMO | E (eV) | −1.380 | −1.523 | −1.641 | −1.657 | −1.783 |
| | Sym | b | b | b | b | b |
| HOMO | E (eV) | −4.432 | −4.340 | −4.243 | −4.270 | −4.195 |
| | Sym | a | b | a | a | a |
| HOMO-1 | E (eV) | −5.064 | −4.341 | −4.243 | −4.298 | −4.195 |
| | Sym | b | a | b | b | b |
| HOMO-2 | E (eV) | −5.222 | −5.239 | −4.838 | −4.533 | −4.624 |
| | Sym | b | b | b | a | a |
| HOMO-3 | E (eV) | −5.973 | −5.256 | −4.838 | −4.533 | −4.625 |
| | Sym | b | a | a | b | b |
| Gap (eV) | | 3.052 | 2.817 | 2.602 | 2.612 | 2.411 |
| Total E (keV) | | −39.3 | −78.6 | −117.9 | −157.2 | −196.5 |
| Dipole (Debye) | | 6.7 | 4.2 | 14.1 | 19.8 | 21.0 |

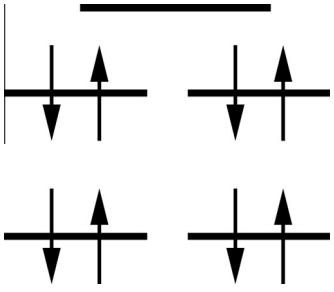

**Fig. 15.** Energy scheme LUMO, HOMO set and HOMO-1 set.

*Computational results*

Fig. 13 shows the sequence followed for the construction of the molecule. We start with a central backbone fragment of dianyline-pyrrole. In step 0 a dianyline-pyrrole fragment is added to the central backbone. From here on, two dianyline-pyrrole fragments are added in each step substituting two $NH_2$, always selecting the external $NH_2$ and keeping the symmetry. Generation 1, 2, 3 and 4 are shown in the same figure. As the molecule grows it shows a helical shape conserving the $C_2$ symmetry for generation 2, 3 and 4. In all cases the steric hindrance was avoided.

The optimized molecule has a central backbone with a rod shape, while the fragments are like wings covering the backbone. As the molecule grows it takes a helical shape. It is expected that the molecules grows in this same way for higher generations. This arrangement resembles the shape of the crystals seen in the microphotographs.

The main feature of this system is focused in the distribution of the frontier molecular orbitals. At generation 0 the LUMO is located at the central backbone with main contributions coming from the p orbitals of the carbons. It has b symmetry and remains the same in the next generations (see Fig. 14). The HOMO is located at the dianyline-pyrrole fragment with irreducible representation a. It is important to note that the next three occupied orbitals are very near in energy but at this step they are not degenerated yet. In fact, the HOMO-1 degenerates with the HOMO from generation 1 to 4. Furthermore, HOMO-2 and HOMO-3 degenerate from generation 2 to 4. These are accidental degenerations since the point group $C_2$ does not have double irreducible representation. The symmetry

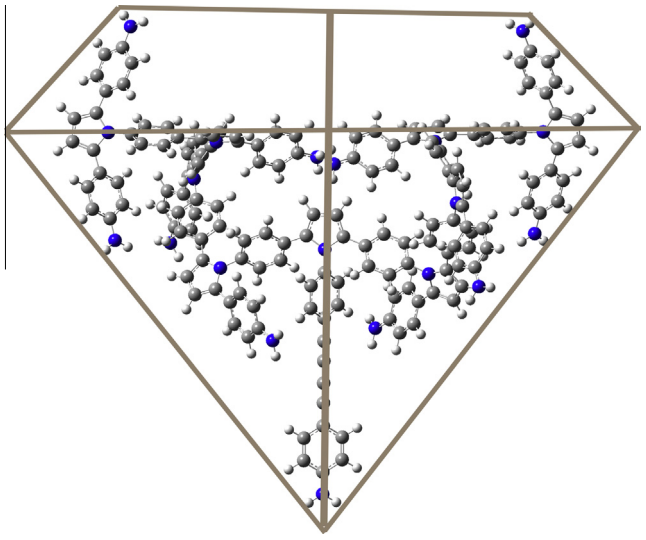

**Fig. 16.** Hyperbranched geometry adjusted by a diamond-like shape with two symmetrical axes.

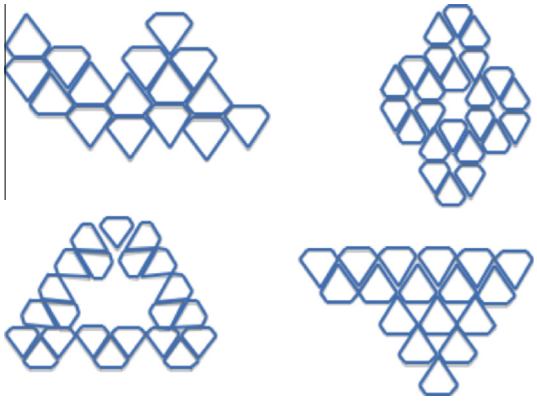

**Fig. 17.** Possible self-assembled macrostructures using as a building block the diamond shape of Fig. 16.

of the LUMO is always b and that of the HOMO is a except for generation 1 that is b. The orbital symmetries do not change from generation 3 to 4 and it is to be expected that will not change for further generations. The energy values and symmetries of the orbitals are given in Table 1. It is important to mention that the total energy is always a multiple of generation 0 total energy.

Fig. 15 shows a scheme of the energy levels in generation 4. The important feature is that the molecule has 8 electrons available to participate in the conducting process since the energy difference between the LUMO and the HOMO and HOMO-1 sets is very small (LUMO–HOMO energy gap 2.41 eV and HOMO, HOMO-1 gap 0.43 eV). This phenomenon is the qualitative explanation of the experimentally measured high conductivity of the samples.

The position of the orbitals is also important since the LUMO is always at the centre of the molecule while the HOMO set is always at the external dianyline-pyrrole fragments. The HOMO-1 set is always located at the fragment of the previous generation. In this way there is an electron flow from the outside to the backbone.

The dipole moment increases with the generation (except for generation 1) but is reaching saturation. It is always aligned with the central bone.

### *Self-assembled phenomena*

We propose a very preliminary theory in which building blocks for the soluble part are the third or fourth generation of the hyperbranched polymer. For example, from our theoretical calculations the structure of the 3rd generation (Fig. 13) could be surrounded by a diamond shape structure to represent steric effects, as is shown in Fig. 16.

By taking this diamond like structure some structures can be formed which resembles the shapes found in the previous photographs, Fig. 12. However, using the diamond like building block and the hyperpolarization characteristics it needs a simulation of the evaporation process by using the diamond like building block and the hyperpolarization characteristics. The high dipole moment will certainly have an important effect in the packing of the structures. It is expected that the antiparallel configuration is the more favorable as shown in Fig. 17.

## Conclusions

Hyperbranched structures containing pyrrole units were obtained from diaminodiphenyldiacetylenes as $AB_2$ type monomers by one-step polymerization.

The para-hyperbranched polymer shows an uncommon symmetry that gives rise to an electronic structure with 8 electrons available to contribute to the high conductivity. It is also important the location of the LUMO at the backbone and of the HOMO sets at the external dianyline-pyrrole fragments. These two features are expected to be conserved, as the molecule grows further and explain the high conductivity observed experimentally.

Conductivity measurements indicated an energy band gap of 0.2 eV, which is 10 times smaller to the theoretical value since the later only considers 4 generations (it is to be expected that the synthetized compounds have hundreds of generations) and does not include the crystalline field found in a solid.

Microscopy studies identify two phases. The first is the insoluble one which gives origin to flake type structures. The second is acetone soluble phase, which generated crystalline structure manifesting in optic anisotropy and rhomboids and triangles dendrimeric structures. Self-assembled process is proposed by using a diamond like structure, however, more work should be done to study this point.

## Acknowledgments

We thank the Computing and Information Technology Division of the UNAM for the computer resources.

## References

[1] M. Seiler, Fluid Phase Equilibr. 241 (2006) 155.
[2] D.A. Tomalia, J.M.J. Frèchet, J. Polym. Sci. Part A: Polym. Chem. 40 (2002) 2719.
[3] S.T. Teertstra, M. Gauthier, Prog. Polym. Sci. 29 (2004) 277.
[4] C.R. Yates, W. Hayes, Eur. Polym. J. 40 (2004) 1257.
[5] C. Gao, D. Yan, Prog. Polym. Sci. 29 (2004) 183.
[6] J. Godínez Sánchez, L. Fomina, L. Rumsh, Polym. Bull. 64 (2010) 761.
[7] L. Fomina, G. Zaragoza Galán, M. Bizarro, J. Godínez Sánchez, I.P. Zaragoza, R. Salcedo, Mater. Chem. Phys. 124 (1) (2012) 257.
[8] G. Huerta-Angeles, L. Fomina, L. Rumsh, M.G. Zolotukhin, Polym. Bull. 57 (2006) 433.
[9] Jorge Godínez Sánchez, Síntesis y caracterización de compuestos hiperramificados con anillos de pirrol obtenidos a partir de diacetilenos, PhD thesis, Universidad Nacional Autonoma de Mexico, Mexico, 2011.
[10] J. Frisch, G. W. Trucks, H. B. Schlegel, G. E. Scuseria, M. A. Robb, J. R. Cheeseman, G. Scalmani, V. Barone, B. Mennucci, G. A. Petersson, H. Nakatsuji, M. Caricato, X. Li, H. P. Hratchian, A. F. Izmaylov, J. Bloino, G. Zheng, J. L. Sonnenberg, M. Hada, M. Ehara, K. Toyota, R. Fukuda, J. Hasegawa, M. Ishida, T. Nakajima, Y. Honda, O. Kitao, H. Nakai, T. Vreven, J. A. Montgomery, Jr., J. E. Peralta, F. Ogliaro, M. Bearpark, J. J. Heyd, E. Brothers, K. N. Kudin, V. N. Staroverov, R. Kobayashi, J. Normand, K. Raghavachari, A. Rendell, J. C. Burant, S. S. Iyengar, J. Tomasi, M. Cossi, N. Rega, J. M. Millam, M. Klene, J. E. Knox, J. B. Cross, V. Bakken, C. Adamo, J. Jaramillo, R. Gomperts, R. E. Stratmann, O. Yazyev, A. J. Austin, R. Cammi, C. Pomelli, J. W. Ochterski, R. L. Martin, K. Morokuma, V. G. Zakrzewski, G. A. Voth, P. Salvador, J. J. Dannenberg, S. Dapprich, A. D. Daniels, O. Farkas, J. B. Foresman, J. V. Ortiz, J. Cioslowskiand D. J. Fox, Gaussian 09, Revision A.02, M., Gaussian Inc, Wallingford CT, 2009.
[11] J.S. Blakemore, Solid State Physics, Cambridge University Press, 1985.